
VIRTUAL PLANE-WAVE IMAGING VIA MARCHENKO REDATUMING

A PREPRINT

Giovanni Angelo Meles

Department of Geoscience and Engineering
Delft University of Technology
The Netherlands
G.A.Meles@tudelft.nl

Kees Wapenaar

Department of Geoscience and Engineering
Delft University of Technology
The Netherlands
C.P.A.Wapenaar@tudelft.nl

Jan Thorbecke

Department of Geoscience and Engineering
Delft University of Technology
The Netherlands
Jan.Thorbecke@tudelft.nl

1 Abstract

Marchenko redatuming is a novel scheme used to retrieve up- and down-going Green's functions in an unknown medium. Marchenko equations are based on reciprocity theorems and are derived on the assumption of the existence of functions exhibiting space-time focusing properties once injected in the subsurface. In contrast to interferometry but similarly to standard migration methods, Marchenko redatuming only requires an estimate of the direct wave from the virtual source (or to the virtual receiver), illumination from only one side of the medium, and no physical sources (or receivers) inside the medium. In this contribution we consider a different time-focusing condition within the frame of Marchenko redatuming that leads to the retrieval of virtual plane-wave responses. As a result, it allows multiple-free imaging using only a one-dimensional sampling of the targeted model at a fraction of the computational cost of standard Marchenko schemes. The potential of the new method is demonstrated on 2D synthetic models.

2 Introduction

Marchenko redatuming estimates Green's functions between the earth's surface and arbitrary locations in the subsurface. Differently from seismic interferometry, in Marchenko redatuming no real sources, nor receivers, are required at the chosen subsurface locations (Broggini et al. (2012b) ; Wapenaar et al. (2014)). These Green's functions are evaluated using reciprocity theorems involving so called 'focusing functions', i.e. wavefields which achieve space-time focusing in the subsurface.

In principle, redatumed Green's functions can be used to provide multiple-free images directly (Behura et al. (2014); Brogini et al. (2014)). However, this approach requires as many virtual sources as there are image points in the subsurface. Marchenko redatuming also allows one to perform redatuming of the reflection response from the surface to a finite number of depth levels and to apply standard imaging in between those datum levels (Wapenaar et al. (2014); Ravasi et al. (2016)). In that case, however, the redatumed reflection responses still include internal multiples reverberating below the redatuming level, which again may diminish the quality of resulting images if the distance between the redatuming levels is too large.

Other applications of the Marchenko method include demultiple schemes (Meles et al. (2015, 2016); da Costa Filho et al. (2017b); van der Neut and Wapenaar (2016)), microseismic source localization (Behura et al. (2013); van der Neut et al. (2017)), inversion (van der Neut and Fokkema (2018)) and homogeneous Green's functions retrieval (Urticoechea and Wapenaar (2017); Wapenaar et al. (2018)).

Despite its requirements on the quality of the reflection response (e.g., knowledge and accurate deconvolution of the source wavelet, co-location of sources and receiver and knowledge of the absolute scaling factor of the recorded data) the Marchenko scheme has already been successfully applied to field data (Ravasi et al. (2016); Van Der Neut et al. (2015); Jia et al. (2017); Staring et al. (2017); da Costa Filho et al. (2017a)). Moreover, recent advances have shown how the requirements above can be considerably relaxed by combining the Marchenko equations with a one-way version of the Rayleigh integral representation (Ravasi (2017)).

In this contribution we show how focusing functions associated with virtual plane-wave-responses can be derived by imposing a time-focusing condition in the subsurface which allows the derivation of a new set of Marchenko equations. The virtual plane-wave-responses can be used to efficiently image the subsurface involving only a fraction of virtual-responses as compared to standard Marchenko methods. The proposed method thus stands as an ideal bridge between areal-source methods for primaries (Rietveld et al. (1992)) and the extended virtual-source Marchenko method addressed by Brogini et al. (2012a).

Potential and limitations of the new strategy are illustrated by means of numerical examples.

3 Method and Theory

In this section we briefly introduce reciprocity theorems and use them to derive the coupled Marchenko equations. To simplify our derivations, we will make use of both time and frequency domain expressions. Following standard formalism, we will indicate wavefields in the time and frequency domain as $p(\mathbf{x}, z, t)$ and $\hat{p}(\mathbf{x}, z, \omega)$, respectively.

Reciprocity theorems for one-way flux-normalized wavefields relate up- and down-going wavefield components of two states A and B evaluated at two depths. Convolution and cross-correlation reciprocity theorems can be expressed in the frequency domain as follows (Wapenaar and Grimbergen (1996)):

$$\int_{\Lambda_a} d^2\mathbf{x} \{ \hat{p}_A^+ \hat{p}_B^- - \hat{p}_A^- \hat{p}_B^+ \} = \int_{\Lambda_f} d^2\mathbf{x} \{ \hat{p}_A^+ \hat{p}_B^- - \hat{p}_A^- \hat{p}_B^+ \}, \quad (1)$$

$$\int_{\Lambda_a} d^2\mathbf{x} \{ \hat{p}_A^+ \hat{p}_B^{+*} - \hat{p}_A^- \hat{p}_B^{-*} \} = \int_{\Lambda_f} d^2\mathbf{x} \{ \hat{p}_A^+ \hat{p}_B^{+*} - \hat{p}_A^- \hat{p}_B^{-*} \}, \quad (2)$$

where $*$ is complex conjugation, subscripts A and B relate to the corresponding states, superscripts $+$ and $-$ indicate down- and up-going constituents, and Λ_a and Λ_f stand for two arbitrary depth levels.

Equations (1) and (2) assume that the medium parameters are identical for both states in the volume circumscribed by Λ_a and Λ_f , and that no sources exist between these depth levels. Moreover, while (1) is valid for lossy media, (2) requires the medium to be lossless between the levels Λ_a and Λ_f , thus posing a limitation to the methodology presented here (for an extension to account for dissipation see Slob (2016)). Moreover, evanescent waves are neglected in equation (2).

We will consider Λ_a and Λ_f to be the acquisition surface and a redatuming level, respectively. Moreover, we consider for state A a truncated medium identical to the physical medium above Λ_f and reflection-free below this level, while for state B we choose the physical medium.

We now discuss and define the properties of the wavefield for state A for two different focusing conditions, which we will refer to as f and F .

In standard space-time focusing, it is assumed that the down-going component of the focusing function representing state A, i.e. f_1^+ , satisfies the following focusing condition along Λ_f : $f_1^+(\mathbf{x}, z_f; \mathbf{x}_F, z_f; t) = \delta(t)\delta(\mathbf{x} - \mathbf{x}_F)$, where \mathbf{x}_F, z_f are the coordinates of a focal point in the subsurface (in the frequency domain this becomes: $\forall \omega, \hat{f}_1^+(\mathbf{x}, z_f; \mathbf{x}_F, z_f; \omega) = \delta(\mathbf{x} - \mathbf{x}_F)$). Moreover, since it is assumed that the medium in state A is truncated below Λ_f , no up-going component f_1^- exists along this lower boundary regardless of its properties along Λ_a (Figure 1(a)).

For state B, following the standard approach, we place a point source for a downgoing wavefield at \mathbf{x}_B at depth z_a just above the surface, so that along Λ_a we have $\hat{p}_B^+ = \delta(\mathbf{x} - \mathbf{x}_B)$ and $\hat{p}_B^- = \hat{R}(\mathbf{x}, z_a; \mathbf{x}_B, z_a, \omega)$, where \hat{R} indicates the reflection response of the physical medium at the surface, and on Λ_f we have $p_B^{+/-} = g^{+/-}(\mathbf{x}, z_f; \mathbf{x}_B, z_a, \omega)$, where g^+ and g^- are the down- and up-going parts of the Green's function.

Substituting these definitions into equations (1) and (2) we get:

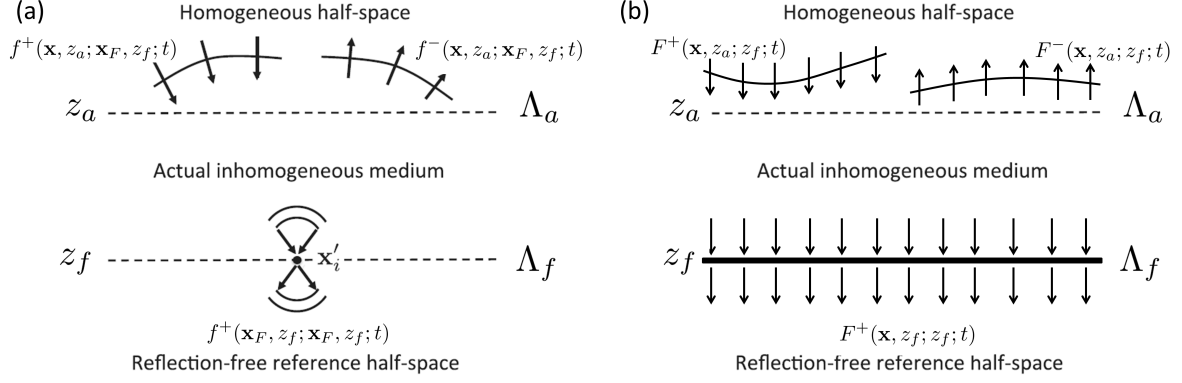


Figure 1: Down- and up-going components of the focusing functions of the 3D wave equation in a reference configuration. (a) Standard space-time focusing function f_1 , leading to point source responses (Green's functions). (b) Time focusing function F_1 , leading to areal-source-responses.

$$\begin{aligned}
 \hat{f}_1^-(\mathbf{x}_B, z_a; \mathbf{x}_F, z_f; \omega) + \hat{g}^-(\mathbf{x}_F, z_f; \mathbf{x}_B, z_a; \omega) &= \\
 \int_{\Lambda_a} d^2\mathbf{x} \hat{R}(\mathbf{x}, z_a; \mathbf{x}_B, z_a; \omega) \hat{f}_1^+(\mathbf{x}, z_a; \mathbf{x}_F, z_f; \omega), \\
 \hat{f}_1^+(\mathbf{x}_B, z_a; \mathbf{x}_F, z_f; \omega) - \hat{g}^{+*}(\mathbf{x}_F, z_f; \mathbf{x}_B, z_a; \omega) &= \\
 \int_{\Lambda_a} d^2\mathbf{x} \hat{R}^*(\mathbf{x}, z_a; \mathbf{x}_B, z_a; \omega) \hat{f}_1^-(\mathbf{x}, z_a; \mathbf{x}_F, z_f; \omega),
 \end{aligned} \tag{3}$$

or, using the compact, time-domain formalism introduced in van der Neut et al. (2015):

$$\begin{aligned}
 \mathbf{f}_1 + \mathbf{g}^- &= \mathbf{R} \mathbf{f}_1^+, \\
 \mathbf{f}_1^+ - \mathbf{g}^{+*} &= \mathbf{R}^* \mathbf{f}_1,
 \end{aligned} \tag{4}$$

where the superscript \star indicates time-reversal.

We now analyze this standard problem in more detail, and show how the algorithm that provides its solution can be easily extended to problems involving different focusing conditions. The underdetermined system in equation (4), which represents the basis for standard Marchenko redatuming, can be additionally simplified invoking a separation operator Θ_f to annihilate the Green's functions terms:

$$\begin{aligned}
 \Theta_f \mathbf{f}_1 &= \Theta_f \mathbf{R} \mathbf{f}_1^+, \\
 \Theta_f \mathbf{f}_1^+ &= \Theta_f \mathbf{R}^* \mathbf{f}_1.
 \end{aligned} \tag{5}$$

This leads, after decomposing the focusing function into a direct and a coda component (i.e., setting $\mathbf{f}_1^+ = \mathbf{f}_{1d}^+ + \mathbf{f}_{1m}^+$, and using $\Theta_f \mathbf{f}_1 = \mathbf{f}_1$ and $\Theta_f \mathbf{f}_1^+ = \mathbf{f}_{1m}^+$), to the invertible linear problem

$$[\mathbf{I} - \Theta_f \mathbf{R}^* \Theta_f \mathbf{R}] \mathbf{f}_{1m}^+ = \Theta_f \mathbf{R}^* \Theta_f \mathbf{f}_{1d}^+, \tag{6}$$

which, under standard convergence conditions (Fokkema and van den Berg (2013)), is solved by:

$$\mathbf{f}_{1m}^+ = \sum_{k=0}^{\infty} (\Theta_f \mathbf{R}^* \Theta_f \mathbf{R})^k \mathbf{f}_{1d}^+. \tag{7}$$

Once the focusing functions are found, they are inserted in equation 4, yielding the point source Green's functions \mathbf{g}^- and \mathbf{g}^{+*} .

More details about the derivation of this series solution can be found in van der Neut et al. (2015), while in Dukalski and de Vos (2017) other algorithms to solve equation (6) are analysed.

We now consider a different focusing condition, which we will refer to as 'time-focusing condition' and show how its imposition results in the same Marchenko equations discussed above. For the time-focusing approach we refer to the focusing wavefield in state A as F_1 . We assume F_1 to be defined in a medium truncated below Λ_f , and therefore also in this case no up-going component F_1^- exists along this lower boundary regardless of its properties along Λ_a . However, differently from the standard space-time focusing approach, we define F_1^+ as satisfying the following time-focusing condition along Λ_f : $\forall \mathbf{x} \in \Lambda_f, F_1^+(\mathbf{x}, z_f; z_f, t) = \delta(t)$, where z_f is the depth of the horizontal focal plane in the subsurface.

Note that in the frequency domain this becomes: $\forall \mathbf{x} \in \Lambda_f, \forall \omega, \hat{F}_1^+(\mathbf{x}, z_f; z_f, \omega) = 1$. Note also that the time-focusing condition can be interpreted as a spatial integral along Λ_f of space-time focusing conditions, namely:

$$F_1^+(\mathbf{x}, z; z_f; t) = \int_{\Lambda_f} d^2 \mathbf{x}_F f_1^+(\mathbf{x}, z; \mathbf{x}_F, z_f; t). \quad (8)$$

It is therefore clear that the focusing function F_1 could be obtained by integrating an appropriate set of focusing functions f_1 , each involving the solution of a Marchenko equation (see equation 7). We will show in the following that the solution of a single Marchenko equation can provide the same result.

For state B we consider again a point source for a downgoing wavefield at \mathbf{x}_B just above the surface.

Substituting these definitions into equations (1) and (2) we get:

$$\begin{aligned} \hat{F}_1^-(\mathbf{x}_B, z_a; z_f; \omega) + \hat{G}^-(z_f; \mathbf{x}_B, z_a; \omega) &= \\ \int_{\Lambda_a} d^2 \mathbf{x} \hat{R}(\mathbf{x}, z_a; \mathbf{x}_B, z_a; \omega) \hat{F}_1^+(\mathbf{x}, z_a; z_f; \omega), \\ \hat{F}_1^+(\mathbf{x}_B, z_a; z_f; \omega) - \hat{G}^{+*}(z_f; \mathbf{x}_B, z_a; \omega) &= \\ \int_{\Lambda_a} d^2 \mathbf{x} \hat{R}^*(\mathbf{x}, z_a; \mathbf{x}_B, z_a; \omega) \hat{F}_1^-(\mathbf{x}, z_a; z_f; \omega). \end{aligned} \quad (9)$$

where

$$\begin{aligned} \hat{G}^-(z_f; \mathbf{x}_B, z_a; \omega) &= \int_{\Lambda_f} d^2 \mathbf{x} \hat{g}^-(\mathbf{x}, z_f; \mathbf{x}_B, z_a; \omega), \\ \hat{G}^{+*}(z_f; \mathbf{x}_B, z_a; \omega) &= \int_{\Lambda_f} d^2 \mathbf{x} \hat{g}^+(\mathbf{x}, z_f; \mathbf{x}_B, z_a; \omega), \end{aligned} \quad (10)$$

or, using again the compact, time-domain formalism:

$$\begin{aligned} \mathbf{F}_1^- + \mathbf{G}^- &= \mathbf{R} \mathbf{F}_1^+, \\ \mathbf{F}_1^+ - \mathbf{G}^{+*} &= \mathbf{R}^* \mathbf{F}_1^-. \end{aligned} \quad (11)$$

Similarly to what considered in equation (4), the set of equations in (11) is also underdetermined. As discussed above, the key ingredient to solve the system in equation (4) is the existence of an appropriate separation operator.

Such an operator does not necessarily exist only for the space-time focusing system (4), as already preliminarily observed in Broggini et al. (2012a) for slightly spatially-extended virtual sources. Here we generalize the observation of Broggini et al. (2012a), now considering plane-wave spatially-extended sources. More precisely, we postulate that when a focusing function \mathbf{F}_1^+ satisfies the time-focusing property discussed above, a separation operator Θ_F (based on the kinematics of the response of $\int_{\Lambda_f} d^2 \mathbf{x} g_d^+(\mathbf{x}, z_f, t; \mathbf{x}', z_a, 0)$, which can be interpreted as a plane-wave source based on reciprocity) can be successfully applied to equation (11).

In this scenario, the existence of a separation operator reduces (11) into:

$$\begin{aligned}\Theta_F \mathbf{F}_1 &= \Theta_F \mathbf{R} \mathbf{F}_1^+, \\ \Theta_F \mathbf{F}_1^+ &= \Theta_F \mathbf{R}^* \mathbf{F}_1.\end{aligned}\tag{12}$$

Following again the decomposition into a direct and coda component of the down-going focusing function, this leads to the solution for the focusing function:

$$\mathbf{F}_1 = \sum_{k=0}^{\infty} (\Theta_F \mathbf{R}^* \Theta_F \mathbf{R})^k \mathbf{F}_{1d}^+.\tag{13}$$

Once the focusing functions are found, they are inserted in equation (11), yielding the plane-wave source Green's functions $\hat{G}^-(z_f; \mathbf{x}_B, z_a; \omega)$ and $\hat{G}^{+*}(z_f; \mathbf{x}_B, z_a; \omega)$. This scheme therefore results in the retrieval of plane wave *up*- and *down*-going areal-receiver-responses (by invoking reciprocity, these responses can be related to the *down*- and *up*-propagating areal-sources-responses discussed in Rietveld et al. (1992)) rather than standard *up*- and *down*-going Green's functions as in van der Neut et al. (2015).

Once these plane-wave-responses are available, they could be used within the areal sources framework (Rietveld et al. (1992)).

4 Numerical Examples

4.1 Focusing performances

We illustrate the potential of the iterative solutions algorithm for areal-sources-responses with Finite Difference examples (Thorbecke et al. (2017)). We consider the 2D inhomogeneous subsurface model in Figure 2.

First we assess the focusing performances of the solution of (7) when a separation operator Θ_F and an initial focusing function \mathbf{F}_{1d}^+ associated with the first arrival of $\int_{\Lambda_f} d^2 \mathbf{x} g^+(\mathbf{x}, z_f; t, \mathbf{x}', z_a; 0)$ are used.

We consider two arbitrarily chosen different depth levels (Lines '1' and '2' in Figure 2). We then solve equation (13) for initial focusing functions \mathbf{F}_{1d}^+ related to the depth levels of Lines '1' and '2', respectively, computing these direct components using the smooth models in Figure 2(c) and (d). The resulting up- and down-going focusing functions are shown in Figure 3. We then inject the retrieved downgoing focusing functions \mathbf{F}_1^+ (Figures 3(a) and (c)) into the corresponding truncated media, and record their response along Lines '1' and '2', respectively.

Figure 4 shows that for both cases the focusing is very good, with only small amplitude artefacts contaminating the wavefield along the focal plane (red arrows in Figure 4). Note that Line '1' crosses an interface, and therefore represents a particularly challenging problem due to the intrinsic limitations of the Marchenko method at interfaces, where the validity of the separation operator can be violated (Vasconcelos et al. (2014)). The overall focusing performances are comparable to those of the standard Marchenko method, shown in Figure (5) for representative points located close to or far-away from interfaces ((a)-(d) in Figure 2), where artefacts (partially due to the finite acquisition aperture) are also seen to contaminate the focusing (red arrows in Figure 5). Note that smooth models (see Figure 2(c) and (d)) were used to initiate the focusing process, and that perfect foci cannot be expected.

Figure 6 compares directly modelled and retrieved Marchenko areal-source-responses at the surface for Lines '1' and '2', respectively. As a direct consequence of the excellent focusing performances demonstrated in Figure 4, the match between the modelled and the retrieved areal-responses is also very good, with mainly tapering-related minor differences in the left- and right-most portions of the gather.

4.2 Imaging results

As mentioned in the introduction, redatumed Green's functions can be used to provide multiple-free images directly, by cross-correlation of up- and direct down-going wavefields in the subsurface (Behura et al. (2014)). However, this approach is expensive, as it requires as many virtual sources as there are image points in the subsurface (number of required Marchenko solutions: $n_x \times n_z$ in 2D, or $n_x \times n_y \times n_z$ in 3D, where n_x , n_y and n_z stand for the number of image points along the x , y and z axis, respectively).

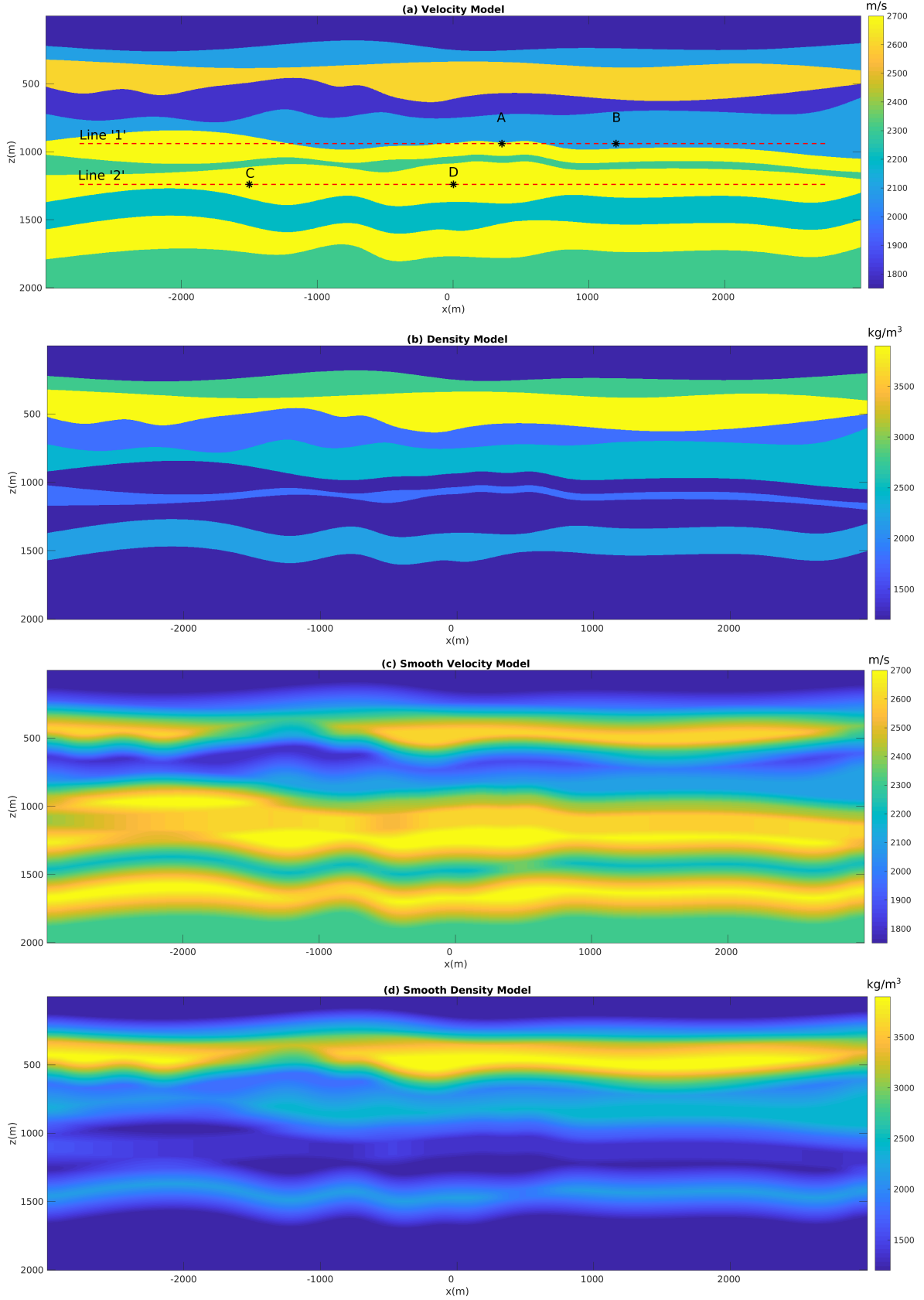


Figure 2: (a) Velocity model used in the first numerical experiment. Dashed lines and stars represents subsurface planes and points for time and space-time focusing, respectively. (b) Density model used in the numerical experiment. (c) and (d) Smooth Velocity and Density models used to provide input for Marchenko redatuming.

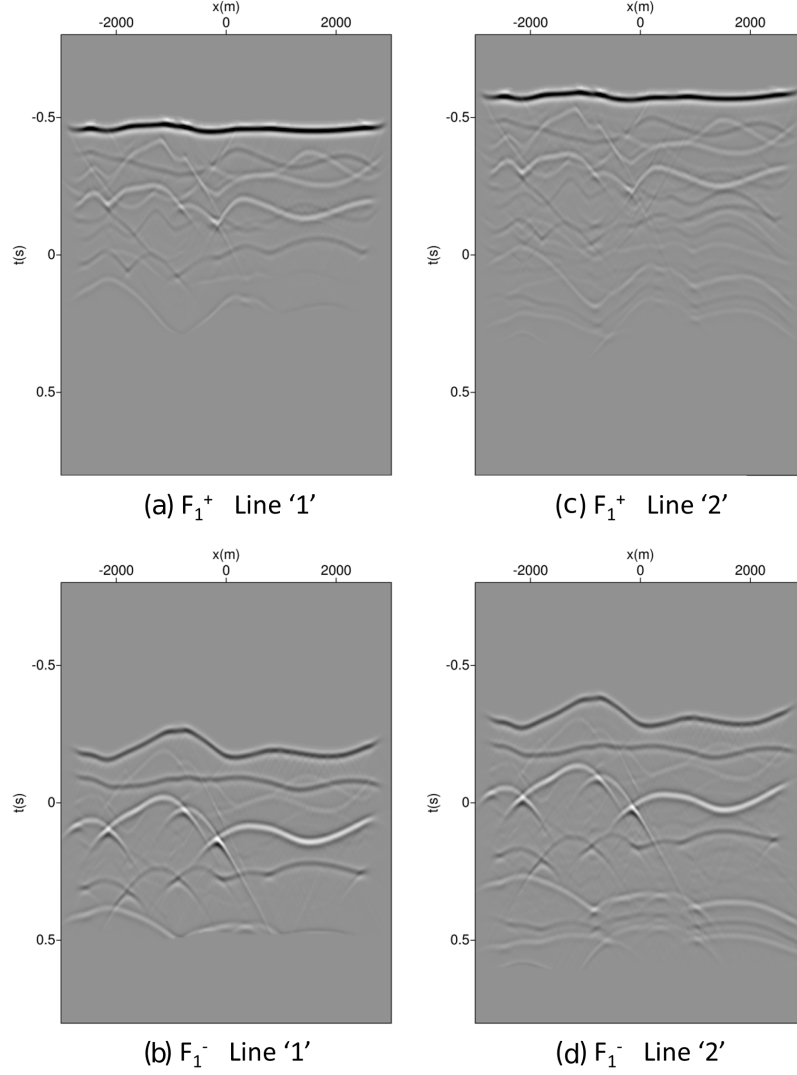


Figure 3: (a) Down-going component of the Focusing function F_1 associated with F_{1d+} being first arrival of $\int_{L_1} d^2 \mathbf{x} g^+(\mathbf{x}, z_f; t, \mathbf{x}', z_a; 0)$. (b) Up-going component of the Focusing function F_1 associated with F_{1d+} being the first arrival of $\int_{L_1} d^2 \mathbf{x} g^+(\mathbf{x}, z_f; t, \mathbf{x}', z_a; 0)$. (c) and (d): as for (a) and (b), but for F_{1d+} associated with the first arrival of $\int_{L_2} d^2 \mathbf{x} g^+(\mathbf{x}, z_f; t, \mathbf{x}', z_a; 0)$.

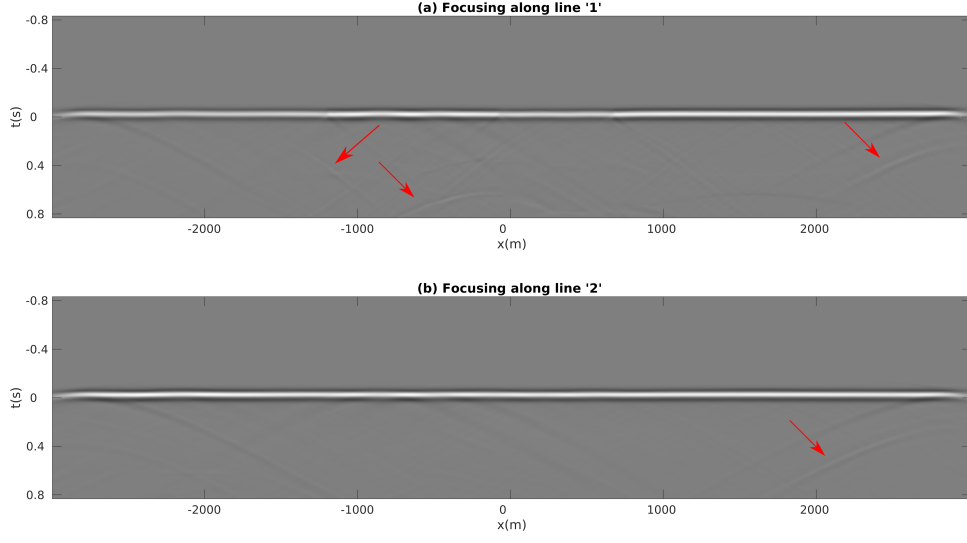


Figure 4: (a) Time-Focusing along Line '1' in Figure 2(a). (b) Time-Focusing along line '2' in Figure 2(a). Red arrows point at small-amplitude artefacts.

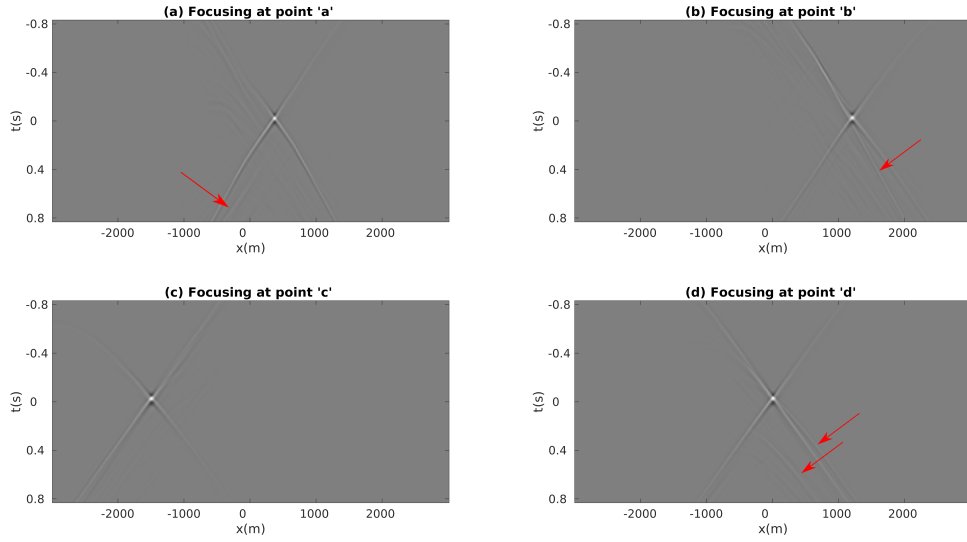


Figure 5: (a) Space-Time Focusing at point 'a' in Figure 2. (b)-(d), as for (a), but for points (b)-(d) in Figure 2. Red arrows point at small-amplitude artefacts.

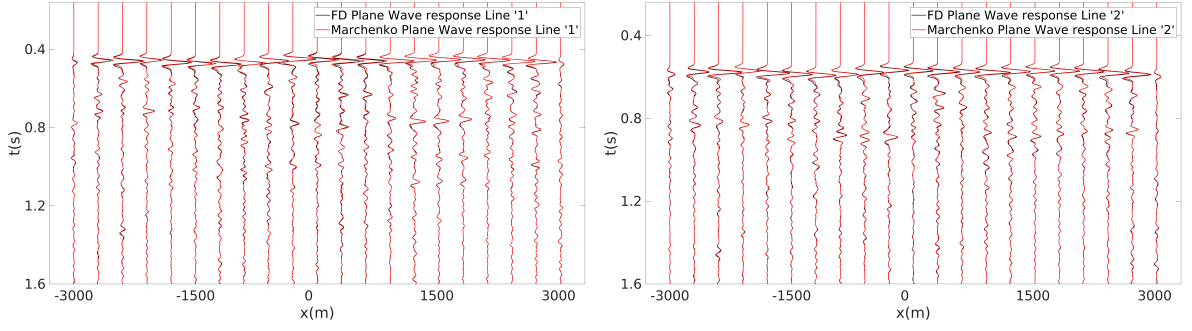


Figure 6: (a) FD modelled (black lines) and Marchenko (red lines) areal source responses for Line '1'. (b) As for (a), but for Line '2'.

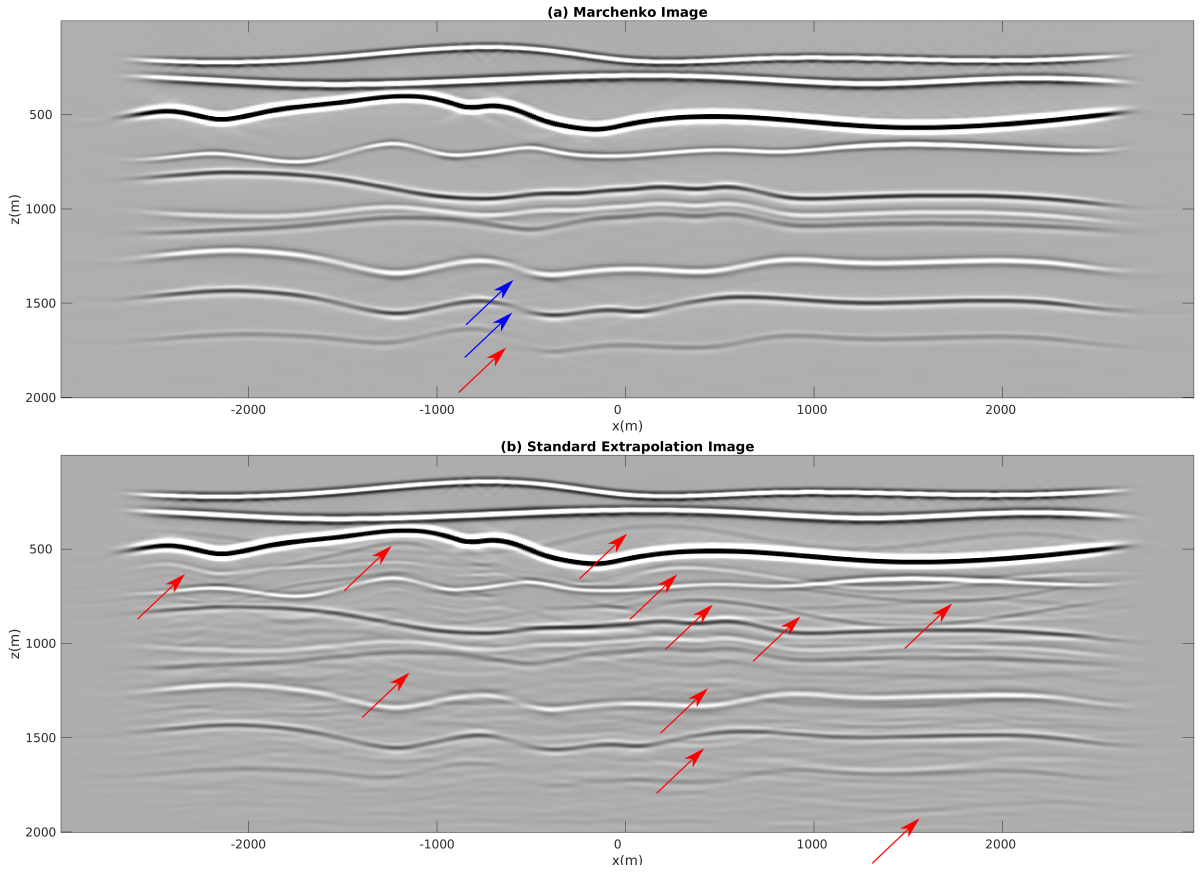


Figure 7: (a) Migration result using the imaging condition of equation (14) and Marchenko redatumed virtual-plane wavefields. The red arrow points at a poorly imaged dipping layer, whereas the blue arrows point at similar structures that are properly imaged. (b) Migration result using standard one-way extrapolation of virtual-plane wavefields. Red arrows point at multiple-related artefacts.

With Marchenko areal-source-responses, however, we can use a single redatumed solution to image a whole line/plane at once (number of required Marchenko solutions: nz in 2D as well as in 3D). To achieve this, we use the following redatumed reflectivity and standard migration imaging condition definitions, in the frequency domain:

$$\begin{aligned}\hat{R}(\mathbf{x}, z_f, \omega) &= \int_{\Lambda_a} d^2\mathbf{x}' \hat{g}_d^{+*}(\mathbf{x}, z_f, \mathbf{x}', z_a, \omega) \hat{G}^-(z_f; \mathbf{x}', z_a, \omega), \\ I(\mathbf{x}, z_f) &= \int_{\mathbb{R}} d\omega \hat{R}(\mathbf{x}, z_f, \omega).\end{aligned}\tag{14}$$

Note that the imaging condition in (14) can be seen as an integral along the focal plane of point sources imaging conditions (this integration is implicit in \hat{G}^-). We expect this integration to reduce the lateral resolution of the final image due to poorer angle-illumination. In the following we will present a strategy to account for this limitation.

We apply our new imaging condition to the model discussed in the previous section. In this case we sample in depth every 5 meters, and consequently to image the entire domain we employ 400 virtual areal sources. Note that imaging the whole model at a 5 meters sampling rate using other Marchenko schemes would involve the computation and migration of up to 400×1200 virtual point-source responses, which would require considerable CPU or RAM resources. An exhaustive analysis about the computational burden of the Marchenko method as an imaging tool can be found in Behura et al. (2014). The migration associated with the imaging condition in equation (14) is shown in Figure 7(a). Each interface is properly imaged, while no multiple-related artefacts are present. Only a dipping layer in the bottom of the model is relatively poorly imaged (red arrow in Figure 7(a)), partially due to its smaller impedance contrast. In any case, others structures with similar geometry are properly imaged (blue arrows in Figure 7(a)). Multiple-related artefacts, on the other hand, contaminate the image if we migrate the up-going response associated with the same areal sources obtained through standard one-way wavefield extrapolation (Figure 7(b)). Note that in the migration step the same smooth models depicted in Figure 2(c) and (d) employed for Marchenko redatuming were used.

We further investigate the potential and limitations of the Marchenko plane wave imaging scheme by considering a more complex subsurface model (Figure 8(a) and (b)). Differently from the medium of the first experiment (Figure 2), the model considered here comprises dipping structures and diffractors. We follow the same imaging strategy discussed for the first numerical experiment, i.e. we initially compute Marchenko areal-source-responses for a set of evenly spaced (sampling every 5 meters in depth) horizontal boundaries and we then apply the redatuming and imaging condition discussed in equation (14). As for the previous experiment, we employ smooth velocity and density distributions both for the Marchenko and migration steps (Figure 8(c) and (d)).

The migration associated with the imaging condition in equation (14) is shown in Figure 9(a). While only minor multiple-related artefacts contaminate the migration result (red arrows in Figure 9(a)), some dipping interfaces are not imaged (red box in Figure 9(a)). However, most structures are properly identified. As for the first experiment, multiple-related artefacts contaminate the image if we migrate standard one-way extrapolated wavefields (red arrows in Figure 9(b)). Blue arrows in Figure 9(a) point at structures clearly visible in the Marchenko image that are partially or totally overshadowed by coherent noise in the standard one-way extrapolation result. Whereas the occurrence of only minor false positives (i.e., multiple-related artefacts) testifies the potential of the method, the presence of false negatives (i.e., the inability to image dipping interfaces) also indicates its limitations. The dipping structures in the red box are not imaged due to the poor illumination provided by horizontal areal-sources. Despite this limitation, the method provides an unexpensive multiple-related free image which could be used to guide more expensive target imaging methods to areas of interests otherwise overshadowed by coherent noise in the standard one-way extrapolation results (such as that of Figure 9(b)).

Moreover, we can improve the imaging results at a small cost by simply employing dipping boundaries in the subsurface and retrieving, via solution of an appropriate Marchenko equation, in- and out-propagating areal-sources-responses associated with tilted planes (the derivation of these new equations is obtained by simply replacing Λ_f in equation (9) with a tilted boundary, and replacing downgoing and upgoing fields by outward and inward propagating fields). The retrieved wavefields provide better illumination of dipping interfaces and therefore improve the overall quality of the migration. To emphasize the benefit of this strategy, we target the area in the red box and employ 4 sets of dipping boundaries (white and black lines in Figure 8(c)). For the geometry considered here, 600 additional Marchenko solutions are used. The same procedure as discussed above, consisting of Marchenko areal-source-response estimation and migration, is then followed. The images associated with horizontal and dipping boundary migrations are finally stacked together and the result is shown in Figure 9(c). While no false positive is

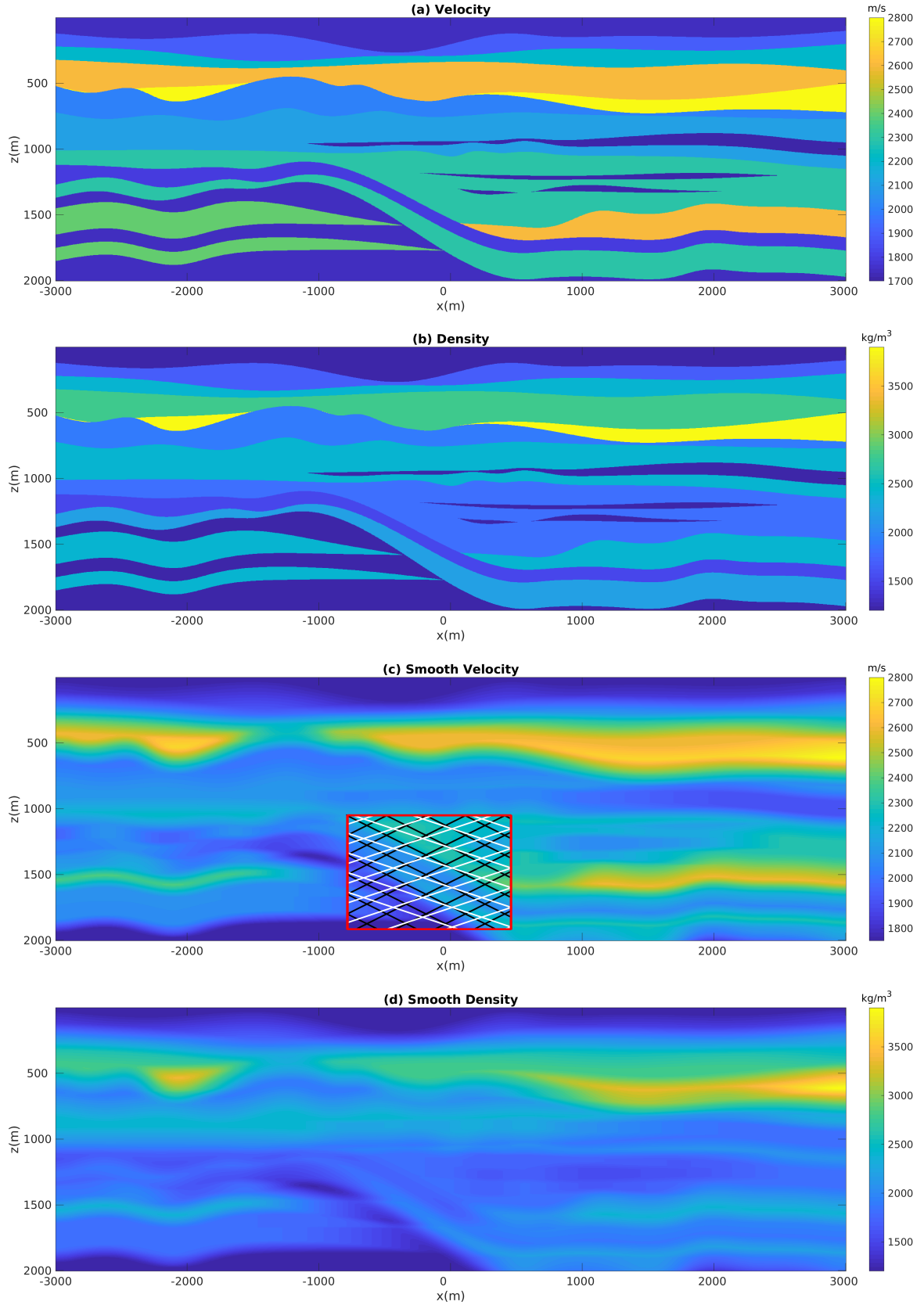


Figure 8: (a) Velocity model used in the second numerical experiment. (b) Density model used in the second numerical experiment. (c) and (d) Smooth Velocity and Density models used to provide input for Marchenko redatuming. The red box in (c) indicates a sub-zone of the model where tilted planes, represented by white and black lines, are used to improve the final imaging result.

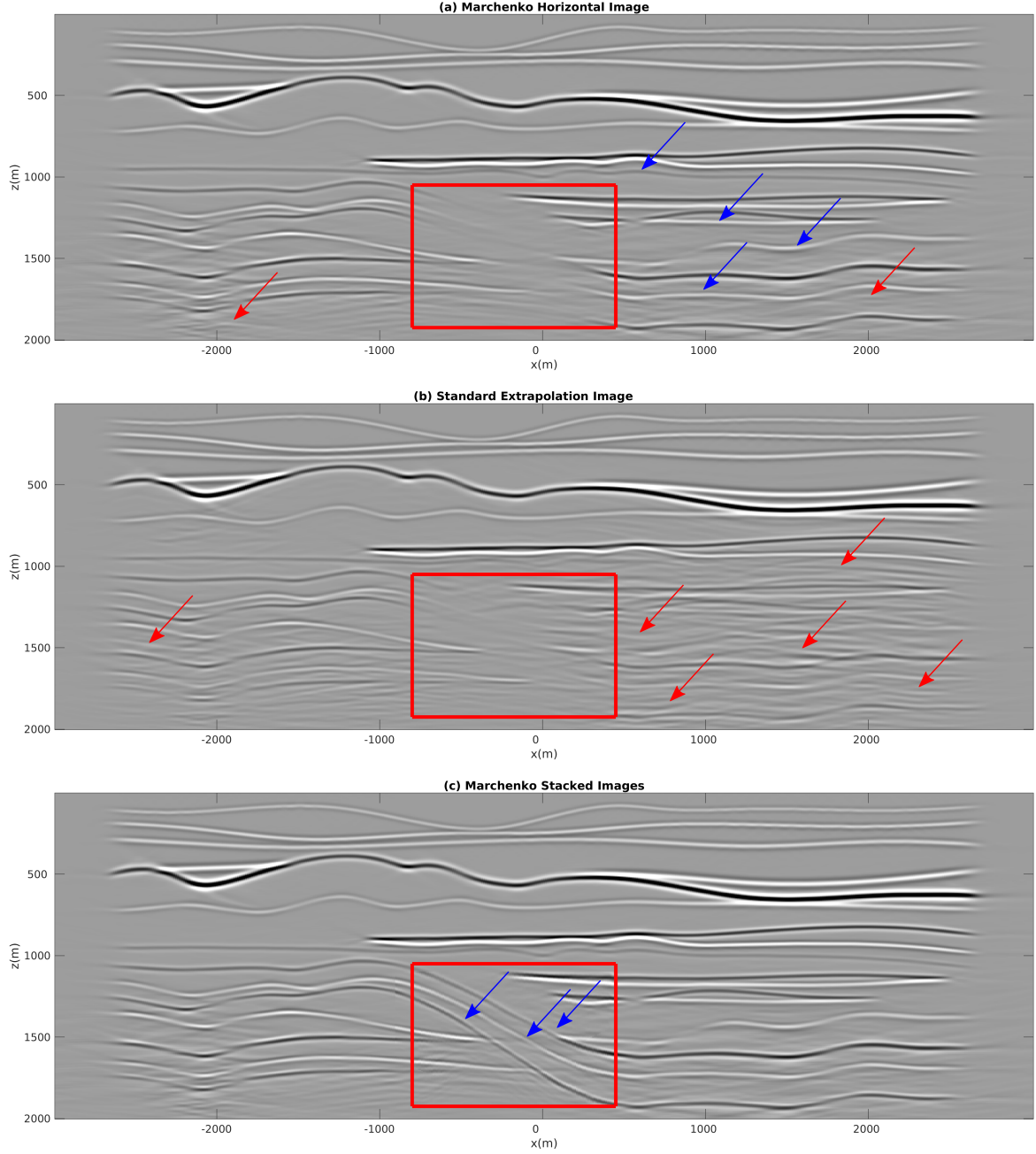


Figure 9: (a) Migration result using the imaging condition of equation (14) and Marchenko redatumed virtual-plane wavefields. The red arrows point at low amplitude artefacts, whereas the blue arrows point at resolved structures not visible in the standard migration image. The red box encircles an area where dipping interfaces are not imaged. (b) Migration result using standard one-way extrapolation of virtual-plane wavefields. Red arrows point at multiple-related artefacts. (c) Migration result using plane wave Marchenko wavefields associated with the tilted planes in Figure 8(c). Blue arrows indicate dipping interfaces now properly imaged.

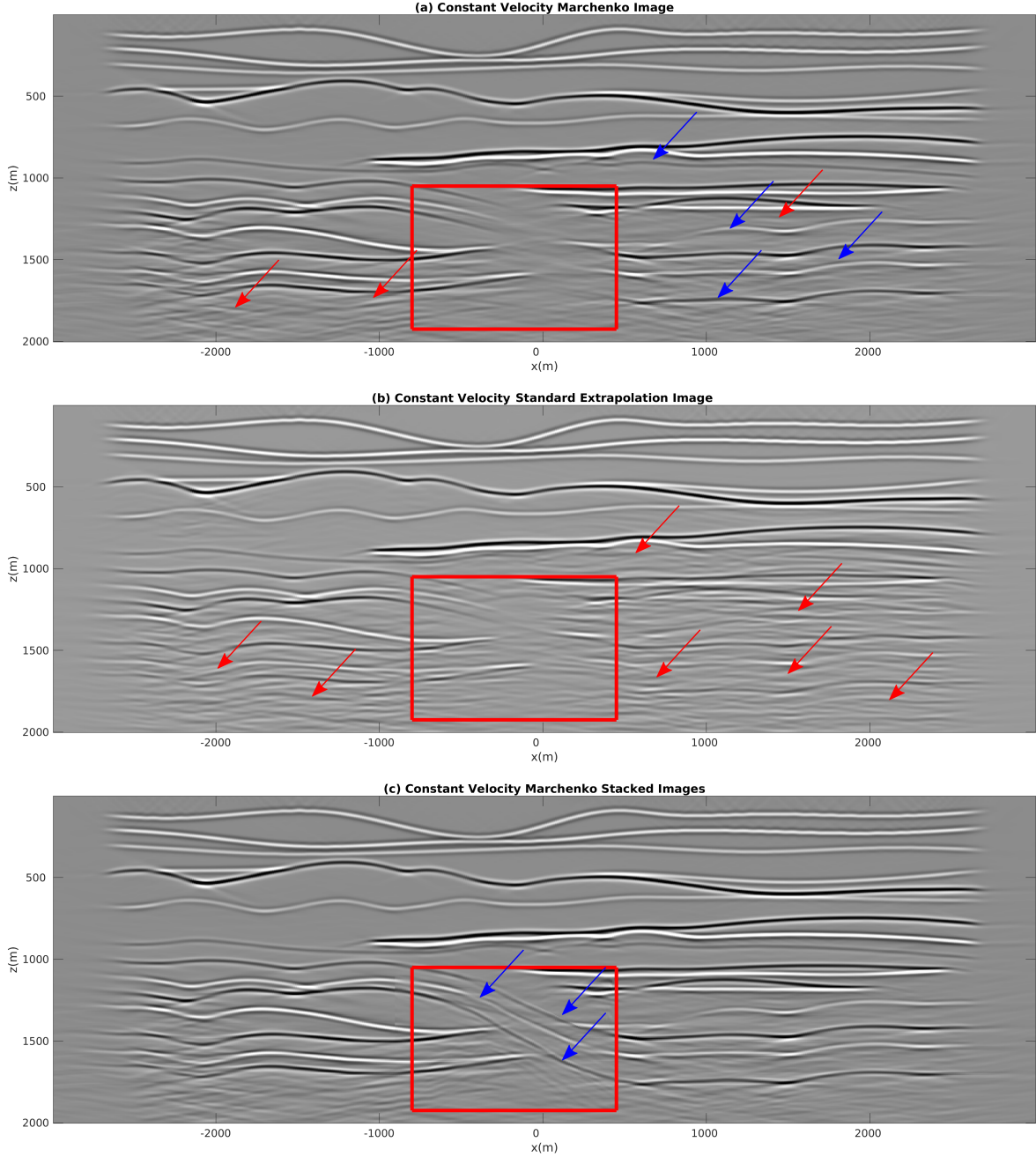


Figure 10: As for Figure (9), but now using a simplified, constant velocity model in the redatuming and migration steps.

contaminating the final image, the previously invisible tilted interfaces are now visible (blue arrows in Figure 9(c)). Consider that the area of the target zone alone is about 1km^2 , which would correspond to about 40000 virtual source locations (at a 5 meters sampling rate) if we chose to image it with other Marchenko schemes. Thus, while involving dipping boundaries increases the computation burden of the areal-source method presented here, its convenience with respect to point-source methods is still significant.

In the examples discussed above we have employed smoothed versions of the actual velocity/density models in the redatuming and migration steps. However, in practical situations it is not always possible to have access to such good

estimates of the true model parameter distributions. To assess the applicability of the method in realistic scenarios we therefore test the Marchenko areal-source scheme also assuming very poor prior knowledge of the actual velocity/density distributions. More specifically, we repeat the second experiment using homogeneous velocity/density models, setting $c = 2000\text{m/s}$ and $\rho = 2000\text{kg/m}^3$. Several authors have already discussed the sensitivity of the Marchenko method to various source of errors (Thorbecke et al. (2013); Meles et al. (2015, 2016); de Ridder et al. (2016)), and here its robustness is further tested. Figure 10(a) shows the migration output corresponding to Marchenko horizontal areal-source-responses. While the image is distorted due to the simplified velocity model employed in the migration step, only minor multiple-related artefacts contaminate the image (red arrows in Figure 10(a)). This demonstrates the good performance of the plane-wave Marchenko method in suppressing standard wavefield extrapolation artefacts even if the employed velocity model is strongly simplified. On the other hand, strong multiple-related artefacts are superimposed to actual interfaces when standard one-way extrapolated wavefields are migrated (red arrows Figure 10(b)). Blue arrows in Figure 10(a) point at structures clearly visible in the Marchenko image that are partially or totally overshadowed by coherent noise in the one-way extrapolation result. As for the previous case, if we include tilted boundaries in the redatuming and migration process, the dipping interfaces are imaged (Figure 10(c)).

5 Conclusions

We have demonstrated that Marchenko methods can be successfully applied beyond conventional space-time focusing. We have discussed how a modified focusing condition relates areal-source-responses associated with horizontal or dipping planes to standard reflection data. A separation operator based on specifically designed direct focusing functions can then be applied to convolution/cross-correlation representation theorems to retrieve areal-source-responses at the surface through standard Marchenko algorithms. The retrieved wavefields can be used to produce images, free of multiple-related artefacts, at a fraction of the cost of standard Marchenko approaches, thus potentially guiding expensive target imaging and being applicable also for 3D data-sets. While more complex problems could deteriorate the performances of the proposed method, the results discussed above demonstrate its applicability to a large class of problems. Analysis and assessment of the resolution properties of the proposed method with respect to standard Marchenko imaging and its extension to elasticity are topics of ongoing research.

6 Acknowledgments

We thank Joost van der Neut, Lele Zhang, Christian Reinicke, Evert Slob, Joeri Brackenhoff and Myrna Staring (Delft University of Technology) for their collaboration and for fruitful discussions which inspired this paper. This work is partly funded by the European Research Council (ERC) under the European Union’s Horizon 2020 research and innovation programme (grant agreement No: 742703). We also thank Nobuaki Fuji and Katrin L  er whose comments have improved the quality of this manuscript.

References

- Behura, J., Snieder, R., et al. (2013). Imaging direct-as well as scattered-events in microseismic data using inverse scattering theory. In *2013 SEG Annual Meeting*. Society of Exploration Geophysicists.
- Behura, J., Wapenaar, K., and Snieder, R. (2014). Autofocus imaging: Image reconstruction based on inverse scattering theory. *Geophysics*, 79(3):A19–A26.
- Broggini, F., Snieder, R., and Wapenaar, K. (2012a). Focusing inside an unknown medium using reflection data with internal multiples: numerical examples for a laterally-varying velocity model, spatially-extended virtual source, and inaccurate direct arrivals. In *SEG Technical Program Expanded Abstracts 2012*, pages 1–5. Society of Exploration Geophysicists.
- Broggini, F., Snieder, R., and Wapenaar, K. (2012b). Focusing the wavefield inside an unknown 1d medium: Beyond seismic interferometry. *Geophysics*, 77(5):A25–A28.
- Broggini, F., Snieder, R., and Wapenaar, K. (2014). Data-driven wavefield focusing and imaging with multidimensional deconvolution: Numerical examples for reflection data with internal multiples. *Geophysics*, 79(3):WA107–WA115.
- da Costa Filho, C., Meles, G., Curtis, A., Ravasi, M., and Kritski, A. (2017a). Imaging strategies using focusing functions with applications to a north sea field. *Geophysical Journal International*, 213(1):561–573.
- da Costa Filho, C. A., Meles, G. A., and Curtis, A. (2017b). Elastic internal multiple analysis and attenuation using marchenko and interferometric methods. *Geophysics*, 82(2):Q1–Q12.

- de Ridder, S., Curtis, A., Van Der Neut, J., Wapenaar, C., et al. (2016). Marchenko wavefield redatuming, imaging conditions, and the effect of model errors. In *2016 SEG International Exposition and Annual Meeting*. Society of Exploration Geophysicists.
- Dukalski, M. and de Vos, K. (2017). Marchenko inversion in a strong scattering regime including surface-related multiples. *Geophysical Journal International*, 212(2):760–776.
- Fokkema, J. T. and van den Berg, P. M. (2013). *Seismic applications of acoustic reciprocity*. Elsevier.
- Jia, X., Guitton, A., Singh, S., Snieder, R., et al. (2017). Subsalt marchenko imaging: A gulf of mexico example. In *2017 SEG International Exposition and Annual Meeting*. Society of Exploration Geophysicists.
- Meles, G. A., Löer, K., Ravasi, M., Curtis, A., and da Costa Filho, C. A. (2015). Internal multiple prediction and removal using Marchenko autofocusing and seismic interferometry. *Geophysics*, 80(1):A7–A11.
- Meles, G. A., Wapenaar, K., and Curtis, A. (2016). Reconstructing the primary reflections in seismic data by Marchenko redatuming and convolutional interferometry. *Geophysics*, 81(2):Q15–Q26.
- Ravasi, M. (2017). Rayleigh-marchenko redatuming for target-oriented, true-amplitude imaging. *Geophysics*, 82(6):S439–S452.
- Ravasi, M., Vasconcelos, I., Kritski, A., Curtis, A., Filho, C. A. d. C., and Meles, G. A. (2016). Target-oriented marchenko imaging of a north sea field. *Geophysical Supplements to the Monthly Notices of the Royal Astronomical Society*, 205(1):99–104.
- Rietveld, W., Berkhout, A., and Wapenaar, C. (1992). Optimum seismic illumination of hydrocarbon reservoirs. *Geophysics*, 57(10):1334–1345.
- Slob, E. (2016). Green’s function retrieval and marchenko imaging in a dissipative acoustic medium. *Physical review letters*, 116(16):164301.
- Staring, M., Pereira, R., Douma, H., van der Neut, J., and Wapenaar, C. (2017). Adaptive double-focusing method for source-receiver marchenko redatuming on field data. In *SEG Technical Program Expanded Abstracts 2017*, pages 4808–4812. Society of Exploration Geophysicists.
- Thorbecke, J., Neut, J. V. D., and Wapenaar, K. (2013). Green’s function retrieval with Marchenko equations: a sensitivity analysis. In *SEG Technical Program Expanded Abstracts 2013*, pages 3888–3893.
- Thorbecke, J., Slob, E., Brackenhoff, J., van der Neut, J., and Wapenaar, K. (2017). Implementation of the marchenko method. *Geophysics*, 82(6):WB29–WB45.
- Urruticoechea, C. R. and Wapenaar, C. (2017). Elastodynamic single-sided homogeneous green’s function representation-theory and examples. In *79th EAGE Conference and Exhibition 2017*.
- van der Neut, J. and Fokkema, J. (2018). One-dimensional marchenko inversion in stretched space. In *Proceedings of the International Workshop on Medical Ultrasound Tomography: 1.-3. Nov. 2017, Speyer, Germany*, page 15. KIT Scientific Publishing.
- van der Neut, J., Johnson, J. L., van Wijk, K., Singh, S., Slob, E., and Wapenaar, K. (2017). A marchenko equation for acoustic inverse source problems. *The Journal of the Acoustical Society of America*, 141(6):4332–4346.
- van der Neut, J., Vasconcelos, I., and Wapenaar, K. (2015). On green’s function retrieval by iterative substitution of the coupled marchenko equations. *Geophysical Journal International*, 203(2):792–813.
- van der Neut, J. and Wapenaar, K. (2016). Adaptive overburden elimination with the multidimensional marchenko equation. *Geophysics*, 81(5):T265–T284.
- Van Der Neut, J., Wapenaar, K., Thorbecke, J., and Slob, E. (2015). Practical challenges in adaptive marchenko imaging. In *SEG Technical Program Expanded Abstracts 2015*, pages 4505–4509. Society of Exploration Geophysicists.
- Vasconcelos, I., van Manen, D., Ravasi, M., Wapenaar, K., and van der Neut, J. (2014). Marchenko redatuming: advantages and limitations in complex media. In *84th SEG annual international meeting, Workshop W-11: Using Multiples as Signal for Imaging*.
- Wapenaar, C. and Grimbergen, J. (1996). Reciprocity theorems for one-way wavefields. *Geophysical Journal International*, 127(1):169–177.
- Wapenaar, K., Brackenhoff, J., Thorbecke, J., van der Neut, J., Slob, E., and Verschuur, E. (2018). Virtual acoustics in inhomogeneous media with single-sided access. *Scientific reports*, 8(1):2497.
- Wapenaar, K., Thorbecke, J., van der Neut, J., Broggini, F., Slob, E., and Snieder, R. (2014). Marchenko imaging. *Geophysics*, 79(3):WA39–WA57.